RSC Advances

PAPER

View Article Online
View Journal | View Issue

Check for updates

Cite this: *RSC Adv.*, 2017, **7**, 42909

Thermal management investigation for lithium-ion battery module with different phase change materials

Ziyuan Wang,[a] Xinxi Li,*[a] Guoqing Zhang,[a] Youfu Lv,[a] Cong Wang,[a] Fengqi He,[a] Chengzhao Yang[b] and Chuxiong Yang[b]

Received 25th July 2017
Accepted 25th August 2017

DOI: 10.1039/c7ra08181b

rsc.li/rsc-advances

Lithium-ion batteries, with their advantages of high energy and power density, have attracted much attention for application in electric vehicles and hybrid electric vehicles. However, there have been increasing reports of lithium-ion batteries catching fire and exploding in recent years, so there is a need for a battery thermal management (BTM) system to ensure battery safety performance. In this study, a novel shaped stabilized structure (paraffin/expanded graphite/epoxy) of composited materials was investigated for the 18 650 batteries module. The selected batteries were evaluated at different conditions to ensure the consistency of batteries initially. Then, different kinds of PCM were applied in the batteries module for thermal management, such as PCM 1 (pure paraffin), PCM 2 (EG 20%, paraffin 80%) and PCM 3 (EG 3%, epoxy 47%, paraffin 50%). The maximum temperatures of the battery modules with PCM 2 decreased more than 10%, 12% and 20% at 1C, 3C and 5C discharge rates, respectively, while paraffin mixed with expanded graphite. Furthermore, PCM can be modified by epoxy: the temperature of the module with PCM 3 was 59.79 °C while that of the module with PCM 2 was 64.79 °C after 30 charge–discharge cycles, revealing that epoxy as a plasticizer can cure the melting paraffin, preventing PCM leakage as the cycle number of the battery increases. The composite materials provide a promising solution to control temperature and decrease temperature difference in batteries modules.

1 Introduction

Traditional vehicles with internal combustion engines contribute about 13% of annual world greenhouse gas (GHG) emissions.[1] Hybrid electric vehicles/electric vehicles (HEV/EV) offer an environmentally friendly alternative, and are emerging as replacements for traditional vehicles in attempts to reduce GHG emissions.[2] Lithium-ion batteries are widely used in HEVs and EVs because of their high gravimetric and volumetric energy density, having advantages over other battery chemistries such as lead acid, nickel metal hydride battery, and others. However, with increasing usage, thermal challenges of lithium-ion batteries have arisen.[3,4] Also, the poor performance at low temperature, degradation of electrodes at high temperature and safety accidents resulting from thermal runaway associated with lithium-ion batteries would have direct influence on performance, cost, reliability, and safety of HEVs and EVs.[5–7] In our previous work,[8] different types of lithium-ion battery were shown to have drawbacks such as overheating and other safety problems, especially at high C-rates, which significantly limited their application. During the charge and discharge process of batteries, the heat is generated consistently as the internal resistance increases,[9–12] with such high temperature conditions influencing the performance of Li-ion batteries.

Overheating can be caused by chemical reaction during the charging and discharging process, especially under high temperature conditions. If the overheating of batteries is not immediately dissipated, thermal runaway can arise, leading to a catastrophic destruction of the batteries.[8,10] The phenomenon is even more significant in large-scale lithium-ion battery packs in which many cells are connected together in series or parallel, as the temperature difference between each cell may cause premature failure of the battery pack and even an explosion or fire in the system.[13] Therefore, a more efficient and less expensive battery thermal management system (BTMS) is essential for battery packs to address the issues of overheating of battery modules and temperature uniformity among different batteries. This would assist in further development of batteries for application in EV/HEV.[13–15]

The main objective of a BTMS is to maintain the battery modules at uniform temperature during operating processes under different environmental conditions, and to improve safety performance and cycling life time. Recently, many studies have concentrated on forced air-based cooling strategies using experimental and simulation methods in different arrangement

[a]School of Materials and Energy, Guangdong University of Technology, Guangzhou 510006, China. E-mail: pkdlxx@163.com

[b]Guangdong Markham Technology Co., Ltd, Shunde 528322, China

structures, which could mitigate temperature rise in the battery directly.[16–20] However, if the temperature rises higher than 66 °C, it would be difficult to cool the batteries below 52 °C by air-cooling. Furthermore, under stressful and abuse conditions, especially at high discharge rates and at high operating or ambient temperatures (>40 °C), air-cooling strategies are not sufficient, and non-uniform distribution of temperature on the surface of the battery becomes inevitable because of the limited heat exchange capability.[30] Liquid-based cooling strategies have also been extensively researched, and are undoubtedly one of the best choices for EVs in high-temperature environments subjected to rapid charge/discharge processes because of their higher thermal conductivity. However, the components of BTMS are extraordinarily complicated, bulky and power-wasting such as pipes and pumps, which can consume the limited energy stored in the batteries.[21–25]

Compared with the two traditional methods of cooling system described, PCM-based cooling strategies appear more suitable because of the stabilized temperature of the phase transition. PCMs have many advantages such as high energy efficiency, high compactness and low maintenance cost, and have drawn great attention in passive thermal management.[26,27] The effects on the solid–liquid phase change process have been investigated for the purpose of enhancing the heat transfer performance of a paraffin-based BTM system. Results showed that the location of the heating wall had an impact on the melting process.[28] A kind of phase change material board (PCMB) was prepared for use in the thermal management of electronics, with paraffin and expanded graphite as the phase change material and matrix, respectively. The PCMB displayed a much better cooling effect than natural air cooling.[29] Rao *et al.* operated numerical simulation on commercial rectangular batteries with PCM and concluded that proper proportion of thermal conductivities with a passive thermal management system was necessary.[30] Graphene-enhanced hybrid phase change materials were also researched for thermal management of Li-ion batteries,[31] and it was shown that graphene incorporation increased thermal conductivity of PCM and led to significantly smaller temperature rise in Li-ion batteries. However, although researchers have focused on improving PCM thermal characteristics by composite material technology during the process of phase changing,[32–36] melting and leaking problems have been neglected in PCM studies. Furthermore, little research has considered the aspect of prolonging the service life of PCM, effectively preventing leakage of PCM for battery modules.

In this study, a novel shape stabilized structure (paraffin/expanded graphite) material/epoxy was investigated for the 18 650 battery module. To assess the thermal and electrochemical performance of the batteries, several electrochemical experiments were performed under high temperature conditions. The heat generation of batteries was obtained through experiments to ensure the accuracy on which the composited material (paraffin/epoxy/expanded graphite) was based. Moreover, PCM 1 (pure paraffin), PCM 2 (EG 20%, paraffin 80%) and PCM 3 (EG 3%, epoxy 47%, paraffin 50%) were prepared and tested by DSC, TGA and thermal cycle tests. We also studied the temperature controlling effectiveness of battery modules with the composited PCMs using a mixed charge–discharge test and charge–discharge cycle test. Finally, the thermal performance and cycle life of PCM 2 and PCM 3 are discussed in depth.

2 Methods

2.1 Governing equations

The active materials in both electrodes (positive and negative) are important for the lithium content of the lithium-ion battery. Lithium-ions can be removed from or inserted into the active material particles without obvious changes in the structure of the electrode. This exchange process is the basis course of lithium-ion batteries. During the charging process, lithium-ion is removed from the active side in the positive electrode and inserted into the negative electrode. Heat generation inside the battery is a complex process and is dependent on the electrochemical reaction rates. It also changes with time and temperature.[37] The x, y, z coordinates of battery heat flux can be evaluated as follows, on the basis of the complex characteristics of its orthotropic materials while charging or discharging:[8]

$$q_x = -\lambda_{xx}\frac{\partial T}{\partial x} - \lambda_{xy}\frac{\partial T}{\partial y} - \lambda_{xz}\frac{\partial T}{\partial z} \tag{1}$$

$$q_y = -\lambda_{yx}\frac{\partial T}{\partial x} - \lambda_{yy}\frac{\partial T}{\partial y} - \lambda_{yz}\frac{\partial T}{\partial z} \tag{2}$$

$$q_z = -\lambda_{zx}\frac{\partial T}{\partial x} - \lambda_{zy}\frac{\partial T}{\partial y} - \lambda_{zz}\frac{\partial T}{\partial z} \tag{3}$$

The energy conservation equation of the battery cell is given by:[38]

$$\rho_b C_b \frac{\partial T_b}{\partial t} = \frac{\partial}{\partial x}\left(k_x\frac{\partial T_b}{\partial x}\right) + \frac{\partial}{\partial y}\left(k_y\frac{\partial T_b}{\partial y}\right) + \frac{\partial}{\partial z}\left(k_z\frac{\partial T_b}{\partial z}\right) + Q_b \tag{4}$$

Assuming a binary electrolyte and neglecting the enthalpy of mixing and phase change effects, the heat generation over all reactions can be expressed as:[39]

$$q = \sum_j \alpha_{sj} i_{nj}\left(\varphi_s - \varphi_e - U_j\right) + \sum_j \alpha_{sj} i_{nj} T\frac{\partial U_j}{\partial T} + \sigma^{eff}\nabla\varphi_s\nabla\varphi_s + \kappa^{eff}\nabla\varphi_e\nabla\varphi_e + \kappa_D^{eff}\nabla\ln\ c_e\nabla\varphi_e \tag{5}$$

The heat balance eqn (6) shows the heat production of a battery cell, including reversible and irreversible heat generation, convection and radiation.[40]

$$mC_p\frac{dT}{dt} = V_t I(t) - \frac{I(t)T\Delta S(t)}{nF} - hA(T - T_a) - \sigma\varepsilon A\left(T^4 - T_a^{\ 4}\right) \tag{6}$$

2.2 Experimental method

A schematic diagram of the experimental system is given in Fig. 1. In the experimental work, initially, several 18 650

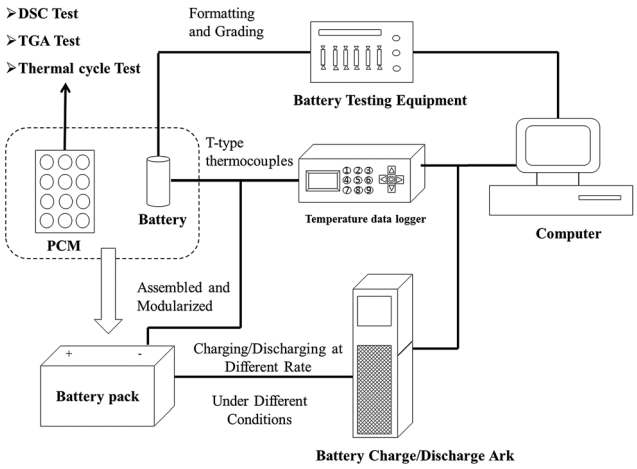

Fig. 1 Schematic diagram of the experimental system.

batteries were formatted and graded by electrochemical testing equipment, and then 20 batteries were selected according to the positive conformity of OCV, ohmic resistance and capacity. The electrochemical performances of the selected batteries, such as DCIR, charge/discharge, cycle and storage tests, were operated with related devices under ambient/high temperature conditions. Thirdly, based on the heat production analysis of 18 650 batteries, a novel shape stabilized structure (paraffin/epoxy/expanded graphite) material was proposed and the thermal performance was analyzed by DSC, TGA and thermal cycle tests. Lastly, the battery charge/discharge ark and temperature data logger were operated to research the thermal and electrochemical performance of the 18 650 battery modules under different conditions.

3 Results and discussions

3.1 Electrochemical analysis of the 18 650 power battery

3.1.1 OCV, ohmic resistance and capacity test of 18 650 cells. Several 18 650 batteries were formatted and graded by electrochemical testing equipment, and 20 were selected and numbered randomly. The fundamental measurement results of OCV (open circuit voltage) and ohmic resistance are listed in Table 1. These highlight the excellent performance of the battery module.

3.1.2 DCIR tests of 18 650 batteries. DCIR (direct current internal resistance) is one of the most important specifications for battery module technology. For DCIR analysis, a test of DCIR under different SOC (state of charge) was executed by a 2–10 A test. During the procedure, the battery was also initially charged in constant current mode at 0.33C rate until it reached a different SOC level. After holding for 120 min, the battery was then discharged at 2 A for 1 s and 10 A for 1 s. After holding 5 s, the same cycle was repeated six times. The equation is given below:

$$\mathrm{DCIR} = \frac{V_{2A1} - V_{10A0}}{\Delta I} \tag{7}$$

Table 1 OCV, ohmic resistance and capacity of individual batteries

Number	OCV (v)	Resistance (mΩ)	Capacity (mAh)
1#	17.8	3.251	2290
2#	18	3.255	2295
3#	17.9	3.27	2281
4#	17.8	3.262	2299
5#	17.9	3.255	2281
6#	17.4	3.258	2281
7#	17.6	3.277	2278
8#	18.2	3.278	2290
9#	17.9	3.236	2277
10#	17.5	3.236	2286
11#	17.7	3.244	2280
12#	17.7	3.238	2279
13#	17.4	3.27	2291
14#	17.9	3.264	2293
15#	17.8	3.278	2286
16#	18.1	3.239	2291
17#	17.6	3.243	2278
18#	18.2	3.242	2289
19#	17.9	3.240	2288
20#	18	3.268	2289

The results of the 2–10 A tests show little variation in DCIR within an SOC range of 10% to 100%, which was positive for electrochemical performance (Fig. 2).

3.1.3 Analysis of storage performance under high temperature. Before the storage test, the selected 18 650 batteries were initially charged in constant current density at 0.5C rate with a terminal cut-off voltage of 4.15 V, and then charged at constant voltage until the current dropped to 0.05 A. After holding for 30 min, the cells were placed in an incubator for 30 days under different temperature conditions. Fig. 3(a) shows that there was little capacity loss from the selected batteries after the storage test. However, as the operating temperature (25 °C, 45 °C, 55 °C, 65 °C and 75 °C) increased, the capacity slowly decreased correspondingly. The largest capacity loss, of 217 mA h, was seen in the selected cell at 75 °C. Fig. 3(b) shows

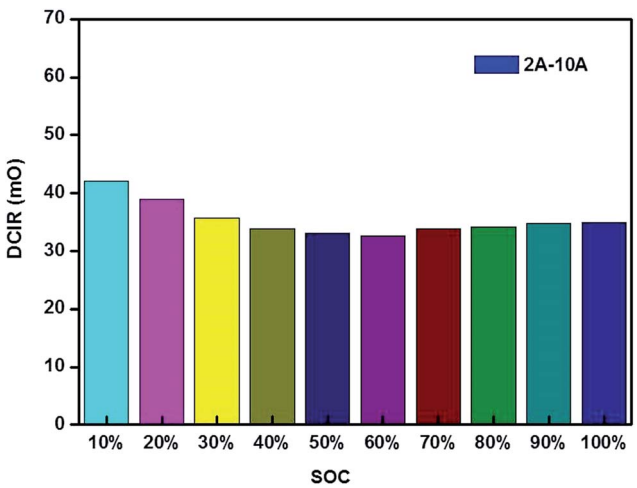

Fig. 2 2–10 A tests of DCIR under different SOC (state of charge).

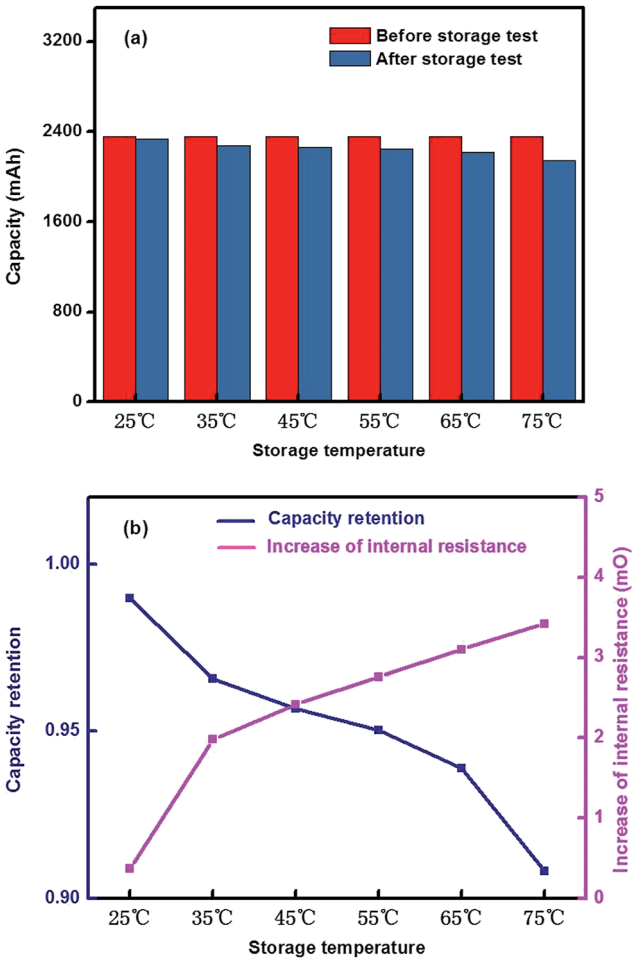

Fig. 3 Storage test under different temperature conditions (a) capacity (b) capacity retention.

that the storage temperature and time could significantly influence the capacity retention and internal resistance. When the temperature was increasing, the capacity retention showed a declining tendency. In other words, the resistance becomes higher as the surrounding temperature is elevated. The higher the storage temperature was, the greater the resistance became. An internal resistance increase of 3.24 mΩ was seen in the selected cell at 75 °C, indicating that the capacity of 18 650 batteries with full charge of energy still declined under high temperature storage conditions. In addition, the internal resistance increased sharply, which could impact the normal operation of power batteries.

3.1.4 Analysis of battery charge–discharge cycle test comparison under ambient and high temperatures. Six 18 650 cells were measured during charge–discharge cycles corresponding to six different temperature (25 °C, 35 °C, 45 °C, 55 °C, 65 °C and 75 °C). During the cycling procedure, the 18 650 cells were initially charged in constant current density mode at 1C rate with a terminal cut-off voltage of 4.15 V, and then discharged in constant voltage until the current dropped to 0.11 A. After holding for 600 s, the cells were then discharged in constant current density at 1C rate until the terminal voltage reached 3.0 V. The final step of the cycle was a resting period of 600 s.

The integrity test steps were repeated 100 times, and the results are displayed in Fig. 4. The capacity of the selected cells showed a declining tendency with increasing cycle number. When the battery number reached the 100th cycle, the worst capacity retention of 77.29% was seen in the selected battery (at 75 °C). We could draw a conclusion from Fig. 4 that the electrochemical performance declined severely while the 18 650 batteries worked under high temperature conditions. More seriously, thermal runaway could occur if the operating

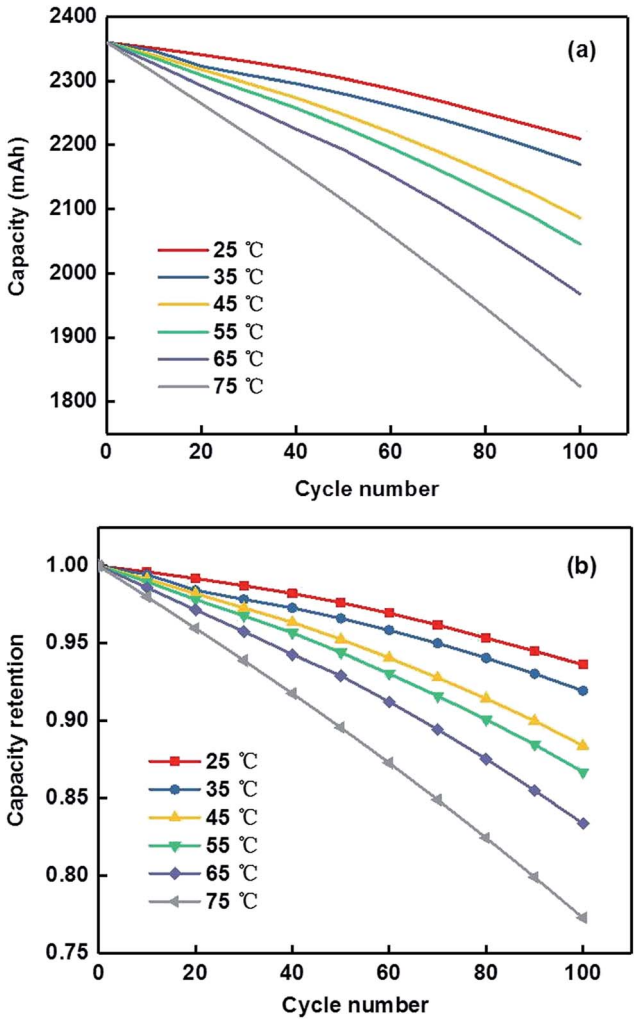

Fig. 4 Battery charge–discharge cycle test under different temperature conditions (a) capacity (b) capacity retention.

Table 2 The electrochemistry parameters of the 18 650 cell

Contents	Parameters
Nominal capacity	2200 mA h
Nominal voltage	3.6 V
Internal resistance	22 mΩ
Discharge cut-off voltage	2.75 V
Charge cut-off voltage	4.2 ± 0.05 V
Nominal charge circuit	0.5C
Maximum charge circuit	5C
Maximum discharge circuit	20 A (<200 ms)

Table 3 The thermal physical parameters of the 18 650 cell

Contents	Parameters
Heat conductivity (x and y coordinates)	1.65 W m^{-1} k^{-1}
Heat conductivity (z coordinate)	1.0 W $m^{-1}\cdot k^{-1}$
Specific heat	5.37 J g^{-1} °C^{-1}
Quality	46 g
Density	2.7786 g cm^{-3}
Diameter	18.4 mm
Height	65 mm

batteries were kept under high temperature conditions for long enough, which would irreversibly influence the battery life. Therefore, it is essential to integrate BTMS into the batteries for controlling the thermal runaway from the battery module, especially under high temperature conditions.

3.2 Heat-transfer analysis of 18 650 power battery using PCM-based cooling management

Considering the above experiments, it can be concluded that 18 650 batteries are impacted seriously by temperature. Furthermore, when the temperature rises to a certain level, the batteries are damaged terribly and thermal runaway can occur. Thus, it is necessary to adopt BTMS for controlling the batteries within safe temperature ranges.

3.2.1 Heat production of the 18 650 single battery. The initial and boundary conditions must be determined precisely and the essential attribute of object should be realized. The parameters of the 18 650 cell are listed in Tables 2 and 3.

The heat production of the 18 650 single battery was evaluated at 1C, 3C and 5C discharge rates, as shown in Fig. 5. The

Table 4 Thermal properties of the composites

Model	Latent heat (J g^{-1})	T_{peak} (°C)	Thermal conductivity (W m^{-1} K^{-1})
PCM 1	245.2	50.32	0.733
PCM 2	148.3	49.89	4.672
PCM 3	123.2	49.71	1.286

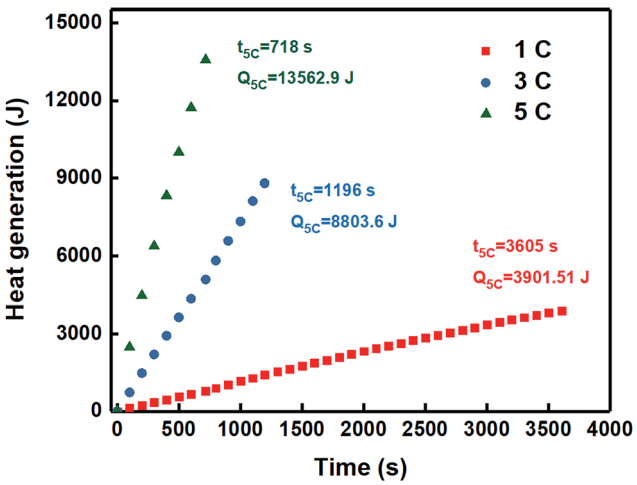

Fig. 5 Heat generation as a function of time for different C rates.

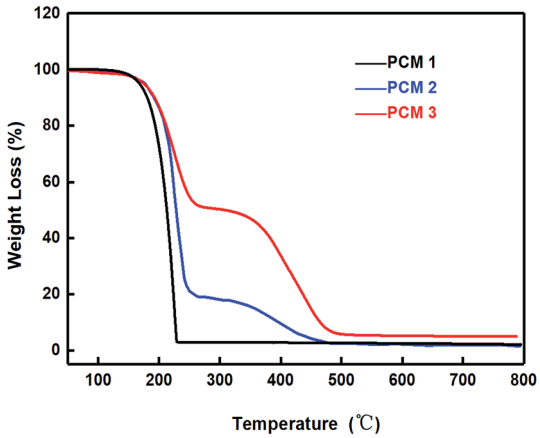

Fig. 7 TGA curves of composite PCMs with various proportions of epoxy.

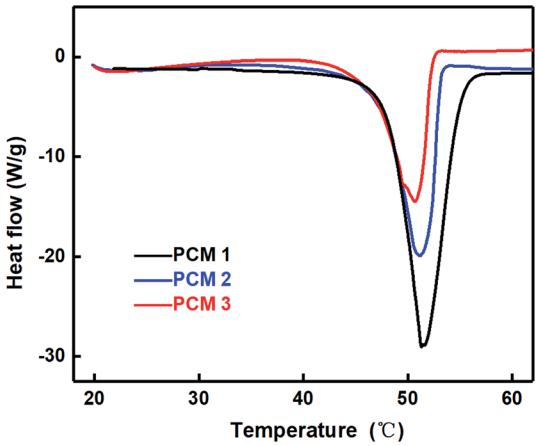

Fig. 6 DSC curves of composite PCMs with various proportions of epoxy.

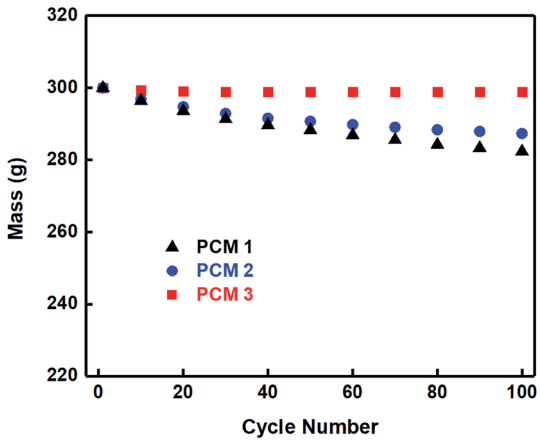

Fig. 8 Thermal cycle curves of composite PCMs with various proportions of paraffin.

results are of relevance to development of BTMS on the basis of different types of PCM.

3.2.2 The thermal behavior of the composited PCMs. Paraffin was adopted as a solid–liquid organic PCM with the advantages of low vapor pressure, high latent heat and chemical stability.[41] However, the leakage of traditional PCM occurs when absorbing heat, which could influence the materials stability. In our previous study, to resolve the leaking and unstable problem of the PCM, expanded graphite (EG) with its high thermal conductivity and porous structure was chosen to improve the thermal performance of composited PCMs. Epoxy was adopted to strengthen the composited PCMs stability because of its excellent thermosetting, highly crosslinked and three-dimensional network.[42]

A novel stabilized material composed of paraffin/epoxy/expanded graphite was fabricated by a sol–gel method at a certain degree temperature, which displayed the melting point of phase change temperature (46–48 °C).[43] The procedure for preparation of the composited PCM is as follows: pure paraffin (PA) was first poured into an aluminum drum at 70 °C until it completely melted to a liquid state. Then, expanded graphite (EG) as porous material with high thermal conductivity was

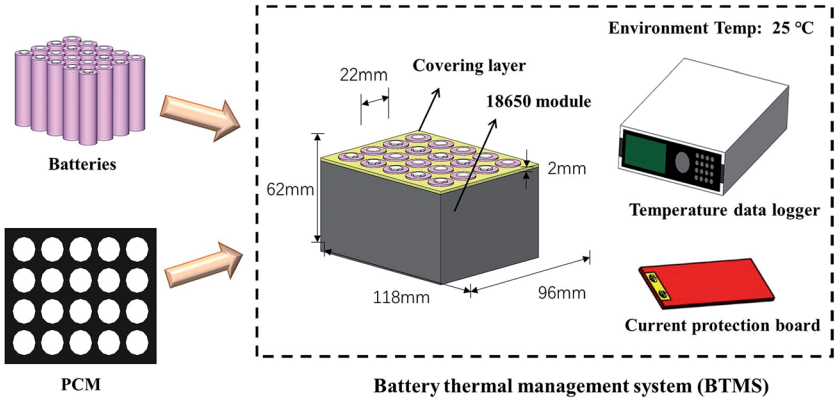

Fig. 9 The battery module composited by selected cells and PCMs.

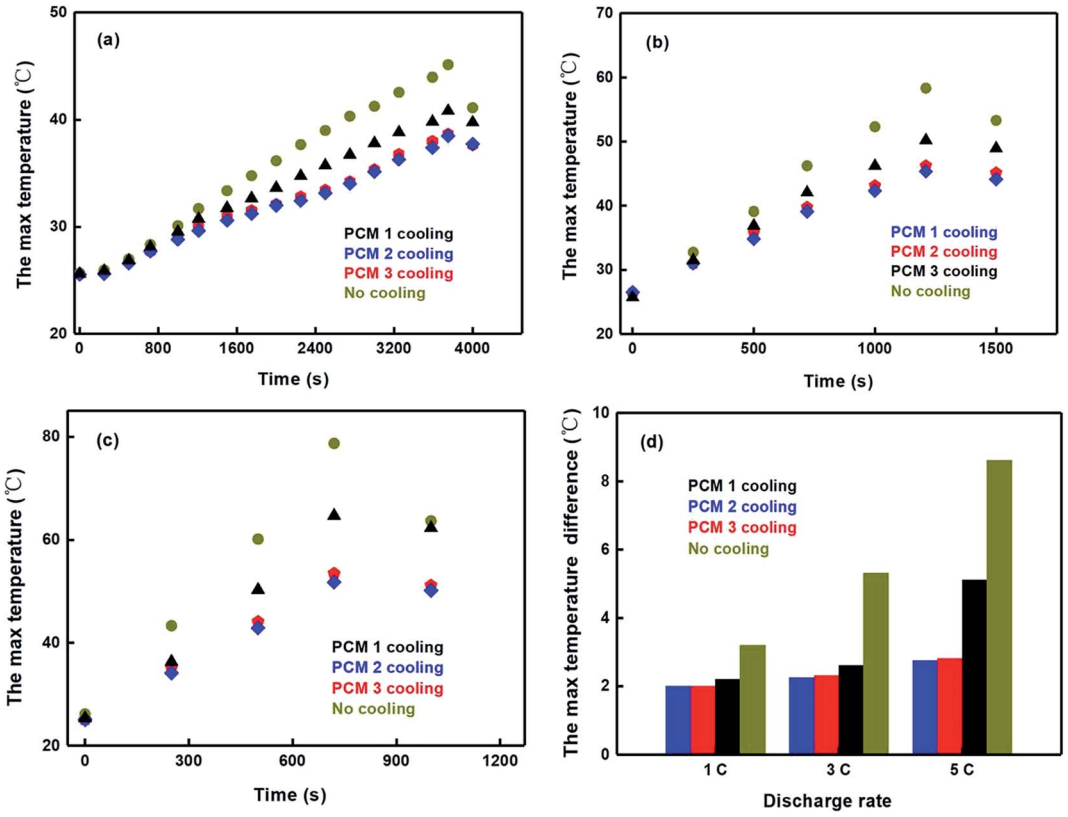

Fig. 10 A mixed charge–discharge test (a) at 1C discharge rate; (b) at 3C discharge rate; (c) at 5C discharge rate; (d) the max temperature difference.

added to the liquid state PA, and a homogenizer was used to disperse the prepared blends at 2000 rad min^{-1} for 0.5 hours (h) to improve the capacity of heat-transfer. Vigorous stirring for 20 min at 70 °C in a water bath was adopted to distribute the three kinds of materials after pouring epoxy into blends, for the purpose of obtaining stable and homogeneous epoxy–paraffin–EG emulsions. Materials with three-dimensional networks can be formed by casting at a high temperature, the melting temperature point between the epoxy and the paraffin, in a calorstat for 24 hours at least.

In this study, PCM 1 (pure paraffin), PCM 2 (EG 20%, paraffin 80%) and PCM 3 (EG 3%, epoxy 47%, paraffin 50%) were prepared, and their thermal properties were measured using a DSC thermal analyzer. The results are shown in Fig. 6 and Table 4. We may draw the conclusion that thermal conductivity of paraffin/epoxy/expanded graphite composites would increase as paraffin content increases, and that fluctuation of T_{peak} value was caused by the plasticization effect of epoxy matrix, which acted as a plasticizer when the paraffin crystallized and melted.

As shown in Fig. 7, in the TGA test the percentage of mass loss changed obviously between 150 °C and 370 °C with different components of PCM, which not only revealed that expanded graphite enhanced the thermal conductivity of composited materials but also that the epoxy could resolve the leakage and unstable problem of PCM. In other words, it can be concluded that pure paraffin is not suitable for thermal cycles, with the main reason being that the paraffin had to liquefy quickly during the absorbing heat process. In addition, the pure paraffin was evaporated when the temperature reached 230 °C, while PCM 2 and PCM 3 can still maintain the state of thermal stability. As shown in Fig. 8, after high-low (55–35 °C) temperature thermal cycle testing for 100 times, 282.336 g of PCM 1 remained, with the worst mass loss of 5.89%. However, the composites PCM 2 and PCM 3 both performed better than PCM 1. In addition, compared with PCM 2 which still showed a mass loss of 4.24%, PCM 3 seldom occurred liquid leakage because of the three-dimensional network structure of epoxy. Considering the results above, PCM 1, PCM 2 and PCM 3 were assembled and modularized with the 18 650 batteries for further study.

3.2.3 The thermal behavior of 18 650 battery modules with PCM-based cooling management. The battery module is shown in Fig. 9, displaying the related current protection board for safety, the covering layer for insulation and T-type thermocouples for temperature collection. The volume of the battery system was fixed and the weights of the PCM 1, PCM 2 and PCM 3 system were 348.26 g, 394.85 g and 367.48 g respectively, according to the known densities. Therefore, the weight percentages of the PCM 1, PCM 2 and PCM 3 systems are 27.25%, 30.03% and 28.54%.

To evaluate the cooling effect on the 18 650 batteries modules, an alternating charge–discharge cycle was carried out. During the experimental procedure, the modules were initially charged in constant current mode at 0.5C rate with a terminal cut-off voltage, and then discharged in constant voltage until the current dropped to 0.1 A. After holding for 60 min, the battery was then discharged in constant current mode at 1C/3C/5C rate until the terminal voltage reached cut-off. The results are shown in Fig. 10. Thus, it can be concluded that the temperature seriously affected the current density. As the discharge rate increases, the temperature of the battery would increase, and the heat production of batteries module would enhance correspondingly.

The maximum temperature of the module with PCM 1 was 40.83 °C, 50.23 °C and 64.69 °C at 1C, 3C and 5C discharge rates separately, which clearly indicate that paraffin exhibited poor heat dissipating performance. In contrast, the maximum temperature of the module with PCM 2 was 38.66 °C, 46.23 °C and 53.43 °C at 1C, 3C and 5C discharge rates separately, and then the maximum temperature of the module with PCM 3 was 38.46 °C, 45.33 °C and 51.73 °C at corresponding discharge rates separately. In addition, the heat dissipating performance of the modules with PCM 2 and PCM 3 displayed similar tendencies because of the expanded graphite which enhanced the thermal conductivity of composite materials. Furthermore, the maximum temperature of the modules with PCM 2 and PCM 3 both decreased more than 10%, 12% and 20% at 1C, 3C and 5C discharge rates, respectively, and the maximum temperature difference of both had to be controlled at less than 3 °C, but the modules with PCM 1 still surpass 5 °C at 5C discharge rate. The main reason is that the excellent thermal conductivity and porous structure of expanded graphite can

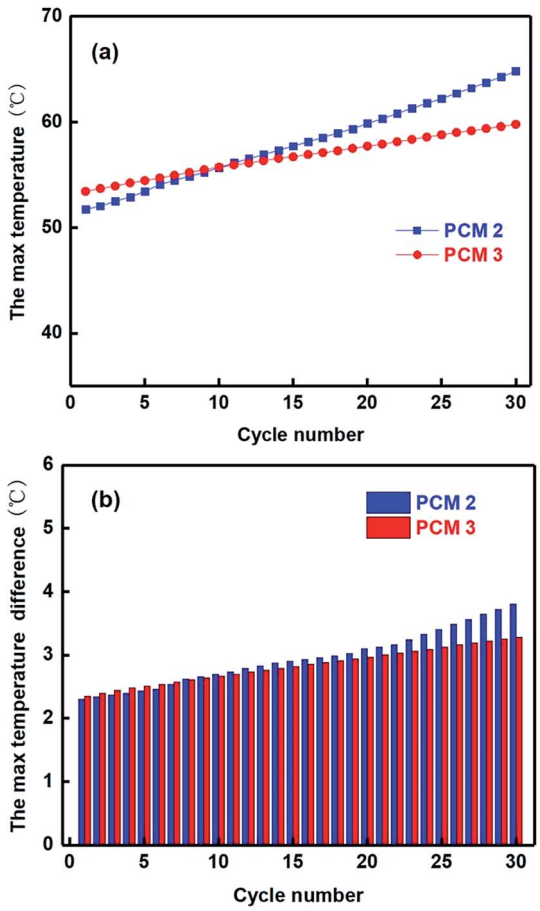

Fig. 11 The charge–discharge cycle test for the modules with PCM 2 and PCM 3 (a) the max temperature of modules; (b) the max temperature difference of modules.

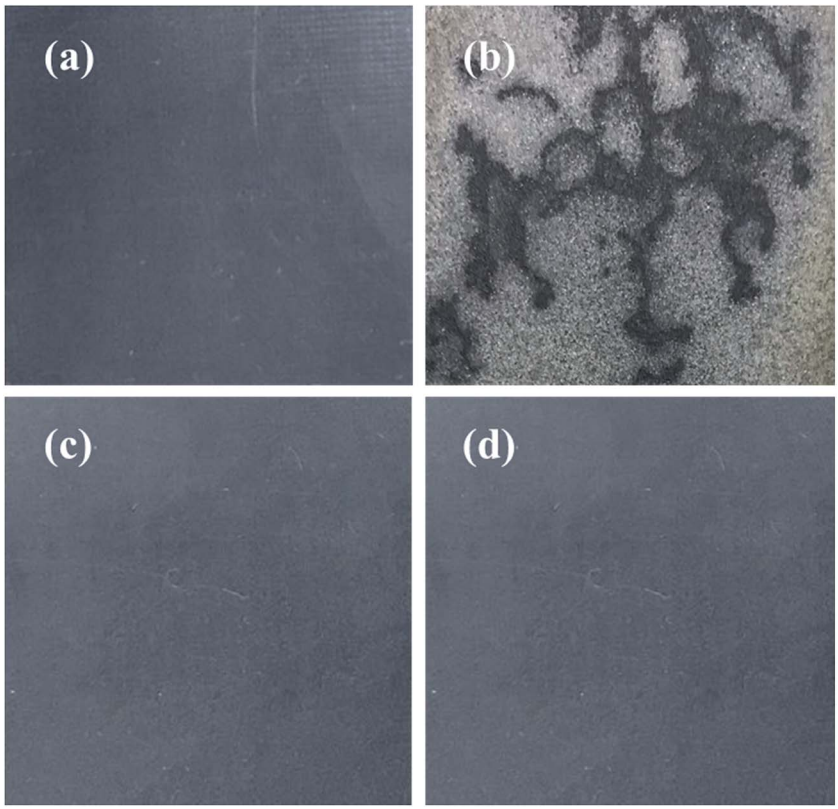

Fig. 12 The surface of PCMs before and after charge–discharge cycle test (a) the surface of PCM 2 before cycle test; (b) the surface of PCM 2 after cycle test; (c) the surface of PCM 3 before cycle test; (d) the surface of PCM 3 after cycle test.

effectively decrease the maximum temperature and temperature difference.

However, in practical applications of batteries, the PCM can easily leak as the charge and discharge cycle increases, so it is necessary to address the problem of leakage of PCMs. During the cycling procedure, the 18 650 batteries module was initially charged at 1C rate, after holding for 600 s, and then discharged at 5C rate, the final step was resting for 1200 s in the first cycle. These steps were repeated 30 times during the cycling procedure, and the experimental results are displayed in Fig. 11. In the first 12 cycles, the temperatures of the module with PCM 2 were lower than the temperatures of the module with PCM 3, which could be attributed to expansion of graphite with high thermal conductivity. However, as the cycle number increased, the max temperature of the module with PCM 2 increased more slowly than that of the module with PCM 3. After the 30th cycle, the temperature of the module with PCM 3 was 59.79 °C while that of the module with PCM 2 was 64.79 °C, and the temperature difference of the module with PCM 3 was maintained at less than 3.3 °C compared with that of module with PCM 2 which reached almost 4 °C. The main reason for this is that the epoxy in PCM 3 can provide a three-dimensional network to stabilize the composite materials and play an important curing role during the paraffin melting process, even though PCM 3 has lower relative thermal conductivity than PCM 2.

To illustrate this phenomenon clearly, an optical picture is presented in Fig. 12 to compare the difference between PCM 2 and PCM 3 before and after 30 cycles. White-veined paraffin appeared irregularly on the surface of PCM 2, revealing that leakage of paraffin occurred as the battery temperature increased until the 30th cycle, shown in Fig. 12(a) and (b). However, the surfaces of PCM 3 showed little difference before and after 30 cycles (Fig. 12(c) and (d)), which could provide excellent thermal management performance for batteries, in particular for improving thermal stability and cycle life. Epoxy contained in PCM 3 can effectively cure the paraffin while the paraffin is melting during the battery charge and discharge process.

4 Conclusions

In this study, a novel shape stabilized structure (paraffin/epoxy/expanded graphite) of composited materials was investigated for the 18 650 batteries module. To research the thermal and electrochemical performance of the batteries, a series of measuring and analysis experiments was designed. The heat generation of selected batteries was evaluated to ensure the consistency of batteries initially. Then, different kinds of PCM were applied in the batteries module for thermal management, such as PCM 1 (pure paraffin), PCM 2 (EG 20%, paraffin 80%) and PCM 3 (EG 3%, epoxy 47%, paraffin 50%), and some conclusions can be summarized as follows:

(1) Paraffin as a phase change material can absorb the heat during the battery charge and discharge process to balance the temperature of the whole battery module.

(2) By adding expanded graphite, the maximum temperature of the battery module with PCM 2 decreased and the temperature difference become smaller than pure paraffin, especially at high discharge rate, with the value reduced more than 10%, 12% and 20% at 1C, 3C and 5C discharge rates, respectively. The main reason for this is that expanded graphite with excellent thermal conductivity can dissipate heat more efficiently than can pure paraffin.

(3) The composite phase change material is further modified by epoxy, the temperature of the module with PCM 3 was 59.79 °C while that of the module with PCM 2 was 64.79 °C after 30 charge–discharge cycles, which can increase the battery module cycle performance because of its three-dimensional structure. Furthermore, epoxy as a plasticizer can cure the melting paraffin and prevent PCM leakage as cycle number of battery increases, thus significantly improving the safety of the battery module.

Conflicts of interest

There are no conflicts to declare.

Nomenclature

q_x	Heat flux in X dimension (J m^{-2} s^{-1})
q_y	Heat flux in Y dimension (J m^{-2} s^{-1})
q_z	Heat flux in Z dimension (J m^{-2} s^{-1})
ρ_b	Density (kg m^{-3})
C_b	Specific heat capacity (J m^{-3} s^{-1})
T_b	Temperature (K)
λ_{xx}	Thermal conductivity in X dimension (W m^{-1} K^{-1})
λ_{xy}	Thermal conductivity in X–Y dimension (W m^{-1} K^{-1})
λ_{xz}	Thermal conductivity in X–Z dimension (W m^{-1} K^{-1})
α_{sj}	Interfacial surface area per unit volume (cm^2 cm^{-3})
σ^{eff}	Effective matrix conductivity (Ω^{-1} cm^{-1})
φ_e	Potential in the solution phase (V)
i_{nj}	Transfer current density (A cm^{-2})

Acknowledgements

This work is supported by Science and Technology Planning Project of Guangdong Province, China (2014B010128001) South Wisdom Valley Innovative Research Team Program (2015CXTD07), Scientific and technological project of Administration of Quality and Technology Supervision of Guangdong Province (2015PJ03), Science and technology application research and development projects of Guangdong Province, China (2015B010135010), Science and Technology Plan Projects of Guangdong Province, China (2016B090918015).

References

1 C. Lan, J. Xu, Y. Qiao and Y. Ma, *Appl. Therm. Eng.*, 2016, **101**, 284–292.
2 J. Jaguemont, L. Boulon and Y. Dubé, *Appl. Energy*, 2016, **164**, 99–114.
3 S. Paul, C. Diegelmann, H. Kabza and W. Tillmetz, *J. Power Sources*, 2013, **239**, 642–650.
4 F. Wu and Z. Rao, *Appl. Therm. Eng.*, 2017, **115**, 659–669.
5 A. Gaitonde, A. Nimmagadda and A. Marconnet, *J. Power Sources*, 2017, **343**, 431–436.
6 K. Chen, X. Yu, C. Tian and J. Wang, *Energy Convers. Manage.*, 2014, **77**, 13–21.
7 P. Han, L. Lu, X. Qiu, Y. Tang and J. Wang, *Energy*, 2015, **91**, 531–539.
8 Z. Wang, X. Li, G. Zhang, Y. Lv, J. He, J. Luo, C. Yang and C. Yang, *RSC Adv.*, 2017, **7**, 27441–27448.
9 R. Spotnitz and J. Franklin, *J. Power Sources*, 2003, **113**, 81–100.
10 B. Koo, P. Goli, A. V. Sumant, P. C. D. S. Claro, T. Rajh, C. S. Johnson, A. A. Balandin and E. V. Shevchenko, *ACS Nano*, 2014, **8**, 7202–7207.
11 C. V. Hémery, F. Pra, J. F. Robin and P. Marty, *J. Power Sources*, 2014, **270**, 349–358.
12 P. Gotcu, W. Pfleging, P. Smyrek and H. J. Seifert, *Phys. Chem. Chem. Phys.*, 2017, **19**, 11920–11930.
13 Y. Azizi and S. M. Sadrameli, *Energy Convers. Manage.*, 2016, **128**, 294–302.
14 R. W. V. Gils, D. Danilov, P. H. L. Notten, M. F. M. Speetjens and H. Nijmeijer, *Energy Convers. Manage.*, 2014, **79**, 9–17.
15 P. Karan, P. Mukhopadhyay and R. Chakraborty, *Energy Convers. Manage.*, 2017, **138**, 577–586.
16 Z. Liu, Y. Wang, J. Zhang and Z. Liu, *Appl. Therm. Eng.*, 2014, **66**, 445–452.
17 H. Park, *J. Power Sources*, 2013, **239**, 30–36.
18 J. Zhao, Z. Rao, Y. Huo, X. Liu and Y. Li, *Appl. Therm. Eng.*, 2015, **85**, 33–43.
19 T. Wang, K. J. Tseng, J. Zhao and Z. Wei, *Appl. Energy*, 2014, **134**, 229–238.
20 S. A. Khateeb, M. M. Farid, J. R. Selman and S. Al-Hallaj, *J. Power Sources*, 2004, **128**, 292–307.
21 Y. Li, H. Q. Xie and J. Li, *Appl. Mech. Mater.*, 2012, **272**, 182–185.
22 J. Zhao, J. Song, B. Zhang, S. Wang and W. Wu, *Automobile Applied Technology*, 2016, **179**, 601–608.
23 T. Zhang, Q. Gao, G. Wang, Y. Gu, Y. Wang, W. Bao and D. Zhang, *Appl. Therm. Eng.*, 2017, **116**, 655–662.
24 T. Wei, K. Somasundaram, E. Birgersson, A. S. Mujumdar and C. Yap, *Int. J. Therm. Sci.*, 2015, **94**, 259–269.
25 X. H. Yang, S. C. Tan and J. Liu, *Energy Convers. Manage.*, 2016, **117**, 577–585.
26 J. Zhao, P. Lv and Z. Rao, *Exp. Therm. Fluid Sci.*, 2017, **82**, 182–188.
27 Z. Rao, Q. Wang and C. Huang, *Appl. Energy*, 2016, **164**, 659–669.
28 Q. Zhang, Y. Huo and Z. Rao, *Science Bulletin*, 2016, **61**, 391–400.
29 W. Wu, G. Zhang, X. Ke, X. Yang, Z. Wang and C. Liu, *Energy Convers. Manage.*, 2015, **101**, 278–284.
30 Z. Rao, S. Wang and G. Zhang, *Energy Convers. Manage.*, 2011, **52**, 3408–3414.
31 P. Goli, S. Legedza, A. Dhar, R. Salgado, J. Renteria and A. A. Balandin, *J. Power Sources*, 2014, **248**, 37–43.

32 B. Mortazavi, H. Yang, F. Mohebbi, G. Cuniberti and T. Rabczuk, *Appl. Energy*, 2017, **202**, 323–334.
33 O. Sanusi, R. Warzoha and A. S. Fleischer, *Int. J. Heat Mass Transfer*, 2011, **54**, 4429–4436.
34 J. N. Shi, M. D. Ger, Y. M. Liu, Y. C. Fan, N. T. Wen, C. K. Lin and N. W. Pu, *Carbon*, 2013, **51**, 365–372.
35 B. Mortazavi and T. Rabczuk, *Carbon*, 2015, **85**, 1–7.
36 X. Liu and Z. Rao, *Thermochim. Acta*, 2017, **647**, 15–21.
37 S. Panchal, R. Khasow, I. Dincer, M. Agelin-Chaab, R. Fraser and M. Fowler, *Appl. Therm. Eng.*, 2017, **122**, 80–90.
38 C. Lan, J. Xu, Y. Qiao and Y. Ma, *Appl. Therm. Eng.*, 2016, **101**, 284–292.
39 Z. Rao, S. Wang, M. Wu, Z. Lin and F. Li, *Energy Convers. Manage.*, 2013, **65**, 92–97.
40 M. S. Rad, D. L. Danilov, M. Baghalha, M. Kazemeini and P. H. L. Notten, *Electrochim. Acta*, 2013, **102**, 183–195.
41 V. D. Cao, S. Pilehvar, C. Salas-Bringas, A. M. Szczotok, J. F. Rodriguez, M. Carmona, N. Al-Manasir and A.-L. Kjøniksen, *Energy Convers. Manage.*, 2017, **133**, 56–66.
42 J. Wei, T. Vo and F. Inam, *RSC Adv.*, 2015, **5**, 73510–73524.
43 Z. Wang, W. Situ, X. Li, G. Zhang, Y. Lv, J. He, Z. Huang, W. Yuan, C. Yang and C. Yang, *Appl. Therm. Eng.*, 2017, **123**, 1006–1012.

